Experiments in Fluids 33 (2002) 405–413
DOI 10.1007/s00348-002-0456-1

Transient high-frequency ultrasonic water atomization

F. Barreras, H. Amaveda, A. Lozano

Abstract An experimental study was performed to improve the understanding of the characteristics of ultrasonic water atomization when excited with waves in the MHz range. In the present experiments, small volumes of water were atomized, observing the temporal evolution of the process. Typical diameters of the resulting droplets are of the order of a few microns. To visualize them, images were acquired with very high magnification. Appropriate lenses were used to enable high resolution at a distance from the flow. Droplet size distributions were also calculated with a Malvern diffractometer. Droplet exit velocity was measured using particle image velocimetry. It was noticeable that, as the remaining liquid mass deposited over the ultrasonic transducer decreased, the atomization characteristics changed, and a second peak of larger droplets appeared in the size distribution function. This phenomenon is related to the change in the curvature of the liquid surface. Although results are not conclusive, it appears that, under the conditions in this study, some observations about droplet formation are better described by cavitation phenomena rather than by the simplified surface wave theory usually invoked to explain these processes.

1 Introduction

Ultrasonic atomization is a very effective way of generating small droplets. Two approaches are common in this context: passing the flow across a standing ultrasonic wave (Bendig 1988) or depositing the liquid over an ultrasonic transducer. The second case originates a fine mist of droplets that are ejected from the transducer at very low velocity. This procedure is going to be studied in the present work and is used, for example, in many commercial humidifiers.

Received: 23 October 2001 / Accepted: 25 February 2002
Published online: 5 June 2002

F. Barreras, A. Lozano (✉)
LITEC/CSIC, Maria de Luna,
10, 50018-Zaragoza, Spain
E-mail: alozano@litec.csic.es

H. Amaveda
Universidad de Zaragoza,
Maria de Luna,
3, 50018-Zaragoza, Spain

This project was partially supported by the Diputación General de Aragón, under contract P104/97. The PIV analysis software was provided by Dr. Julio Soria from Monash University.

The present work is subject to some specific characteristics. First, the atomization is restricted to water. Secondly, the ultrasonic frequencies were selected in the MHz range, because interest was focused on micron-range droplets. Finally, in contrast to most experimental studies reported in the literature, for some measurements discrete water volumes were atomized without supplying a constant flow to keep a fixed liquid level over the transducer. This is why atomization in these experiments has been described as transient. All these conditions are representative of those that would occur if an ultrasonic atomizer were used to administer by inhalation a metered dose of a drug diluted in an aqueous solution. The objective of this work is to study the temporal evolution of the process, and the characteristics of the generated spray.

2 Historical review

The possibility of generating a cloud of droplets by means of ultrasonic waves was first reported by Wood and Loomis (1927). Two different mechanisms have since been invoked to explain the ultrasonic atomization, capillary waves, and cavitation. Scientific publications on the subject can be divided into two groups, with different approaches depending on which one of these mechanisms is considered to be responsible for the spray formation. However, the interaction between them and the limits in which one could predominate over the other depending on the different atomizing situations are still not clear.

The first studies on stationary waves on the free surface of a liquid mass subjected to periodic vertical forcing were reported by Faraday (1831). In 1871, Kelvin derived the well-known equation for capillary waves

$$\lambda = \left(\frac{2\pi\sigma}{\rho f^2}\right)^{1/3} \tag{1}$$

where λ is the wavelength, σ is the surface tension coefficient, ρ is the liquid density, and f is the frequency of the surface waves (Kelvin 1871). This research was continued by Rayleigh (1883), who modified Kelvin's equation and derived the expression

$$\lambda = \left(\frac{8\pi\sigma}{\rho F^2}\right)^{1/3} \tag{2}$$

where F is the forcing sound frequency. It is to be noted that the relation $f=F/2$ was obtained empirically from experimental measurements.

In 1917, Rayleigh described the first mathematical model to explain the bubble collapse in incompressible liquids, in his attempts to explain the physical mechanisms involved in ultrasound propagation in liquids (Rayleigh 1917).

This was the current theoretical basis when Wood and Loomis (1927) discovered the possibility of atomizing liquids by exciting them with ultrasonic waves. An explanation for this process was proposed by Söllner (1936a) based on cavitation produced under the liquid film. However, numerous later works (Bisa et al. 1954; Benjamin and Ursell 1954; Sorokin 1957; Eisenmenger 1959) pointed to unstable surface capillary waves as the origin of the droplet formation, mostly relying on simplified linear instability analysis. In 1962, Lang published detailed experimental research presenting his famous expression relating wavelength to droplet size through an empirical constant k, whose value obtained fitting his experimental measurements was reported to be 0.34, placed in front of Eq. (2) (Lang 1962). His experiments were performed for frequencies up to 800 kHz. A more elaborated theoretical model based on interfacial Taylor instability triggering the surface waves was later developed by Peskin and Raco (1963). Together with the wavelength, they introduced the wave amplitude and the sheet thickness as parameters determining the droplet diameter.

The atomization theory based on cavitation, abandoned during this period, was resumed by Eknadiosyants and coworkers (Gersherson and Eknadiosyants 1964; Eknadiosyants 1968). After these, several studies have tried to combine both theories (Fogler and Timmerhaus 1965; Boguslaskii and Eknadiosyants 1969; Topp 1973; Chiba 1975; Basset and Bright 1976), some of them indicating that the prevalence of each one might depend on the ultrasonic intensity.

These explanations are still subject to controversy, and papers on this topic continue to be published from both experimental (Edwards and Fauve 1994; Sindayihebura et al. 1997) and theoretical (Miles 1994; Sindayihebura and Bolle 1998) approaches.

3
Description of the experiment

Water was atomized, depositing small amounts over an ultrasonic transducer. The transducer, shown in Fig. 1, is formed by a PZT 4 piezoceramic disk with a diameter of 20 mm and a thickness of 1.3 mm. The resonance frequency of this disk was measured to be 1.65 MHz. The disk was excited with a sinusoidal wave coincident with the resonance frequency and variable amplitude. The maximum voltage that could be delivered without damaging the ceramic was 50 V. For voltages below 15 V, no atomization was observed. The atomization process is displayed in Fig. 2a.

To visualize the atomization process, images were acquired with a Princeton Instruments (division of Roper Scientific, Trenton, N.J.) CCD camera. To freeze the motion, the flow was illuminated with 6-ns pulses from a double cavity Quantel (Les Ulis, France) YG781C-10 Nd:YAG laser. The optical system was arranged to operate with high magnification to resolve the small droplets. An

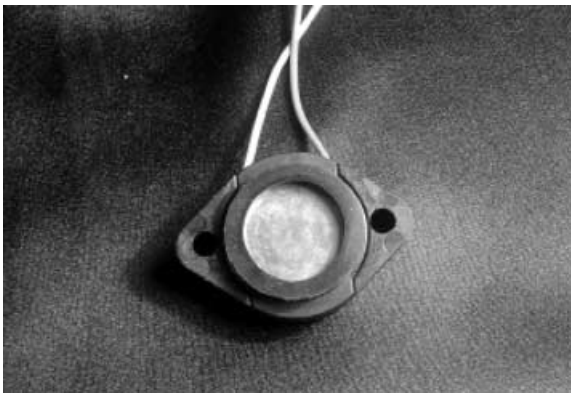

Fig. 1. Image of the piezoceramic disk used in the present experiments

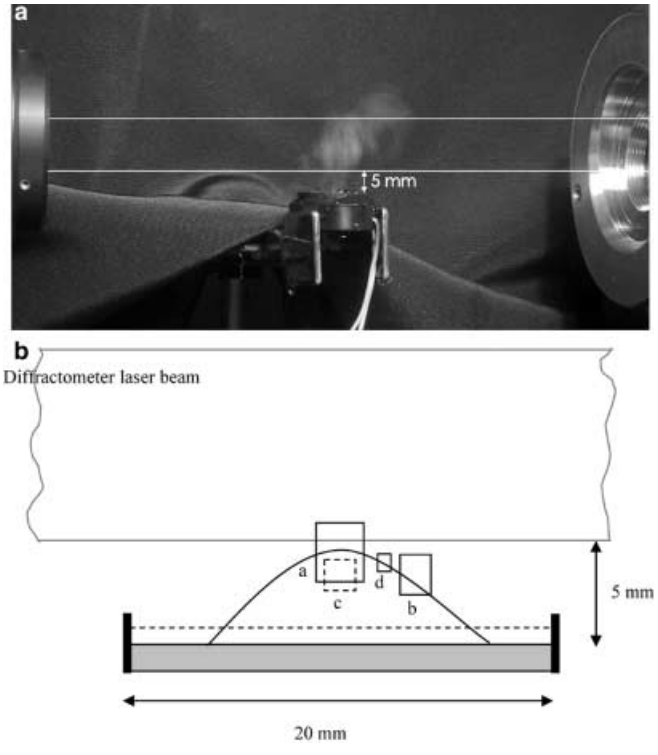

Fig. 2. **a** Image of the disk during the atomization process, with indication of the diffractometer laser beam position. **b** Sketch of the experiment indicating size and approximate location of the different zones registered in the images in this work. Sizes are: *a* 2.9×2.1 mm; *b* 1.45×1.9 mm; *c* 1.5×1.5 mm; *d* 0.5×0.75 mm

inverted 50-mm Nikon (Tokyo, Japan) lens attached to a bellows extension was used, as well as a Questar QM100 telemicroscope (Questar Corporation, New Hope, Pa.). Different areas were imaged with these configurations. They are depicted in Fig. 2b: zone *a* is 2.9×2.1 mm, zone *b* is 1.45×1.9 mm, zone *c* is 1.5×1.5 mm, while zone *d* is 0.5×0.75 mm. A maximum resolution of 2 μm/pixel was achieved. Top and side views of the vibrating disk with water were obtained to observe the liquid surface and the air/water interface. For the side views, the flow was illuminated by a 5-cm-high laser sheet, with a thickness of 0.5 mm. In some cases, to avoid laser reflections, a

fluorescent dye was used (sulforhodamine B) recording the induced emission.

Droplet size distributions were also measured with a Malvern Mastersizer (Malvern Instruments Ltd, Malvern, UK) laser difractometer. The laser beam crossed the spray cloud 5 mm above the transducer surface (see Fig. 2). From the distributions, mean diameters and other statistical parameters were calculated. In particular, bearing in mind that the specific atomization configuration under study is prone to occur in medical drug administration to the respiratory track based on nebulization and inhalation of the resulting aerosol, those parameters more relevant in this situation were studied. Two diameters, D_{10} and D_{30}, were analyzed. Furthermore, some other statistical indicators were also calculated: the 10% and 50% volume percentile $D_{v0.1}$ and $D_{v0.5}$, plus the cumulated volume fraction below 5 μm. This last quantity is especially important because, for a medical metered dose inhaler to be deemed acceptable, it has to satisfy that a minimum mass fraction of the drug solution must be delivered in the form of droplets below a certain maximum diameter, which for some specific applications is taken to be 5 μm.

Velocity measurements were obtained using particle image velocimetry (PIV). 736×736 pixel image pairs of the droplets were registered with a PCO SensiCam camera (PCO Computer Optics GmbH, Kelheim, Germany), with a temporal interval of 200 μs and a spatial resolution of 2 μm/pixel, covering a total field of view of 1.5×1.5 mm (zone *c* in Fig. 2). The same laser and optical configuration used in the flow visualizations were arranged for these measurements. The image pairs were analyzed by cross-correlation with 64-pixel windows iterated in a second pass down to 32-pixel windows displaced in accordance with the mean velocity calculated in the first pass.

4 Experimental results

4.1 Visualizations

For the present experiments the following atomization scenario was observed. After depositing a small amount of water (typically 0.2–0.4 ml) over the piezoceramic disk, and upon excitation with a 1.65-MHz sinusoidal wave, the disk starts vibrating. For voltages below 15 V, no atomization is produced, although a pattern of surface waves can be observed in the liquid interface. This effect is evidenced in Fig. 3, corresponding to a top view of the transducer obtained with a resolution of 12 μm per pixel and covering a field of view of 4.6×3.5 mm. In this case, the excitation amplitude was 15 V. For varying voltages, it was observed that the visible wavelength of the capillary instabilities is approximately constant, in agreement with most theories relating the surface waves to the ultrasonic forcing. The wavelength was estimated to be 0.9 mm, although the appearance of the surface pattern is formed by receded polygons bordered by thinner crests. The width of these crests would be around 100 μm. Applying Rayleigh's relation, Eq. 2, the calculated wavelength value is 8.7 μm, in notorious discrepancy with the visually observed wavelength. There would be a possibility of having a

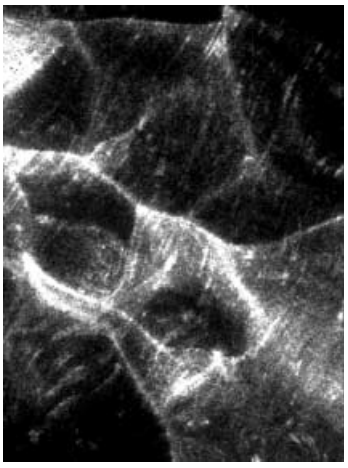

Fig. 3. Top view of the surface waves on the water interface for a forcing voltage of 15 V. Field of view of 4.6×3.5 mm and resolution 12 μm/pixel

superposition of two waves with different spatial frequency. In the present images, the conjectured one with the shorter wavelength has not been observed.

As the voltage is increased, the liquid assumes a conical shape, irrespective of the surface waves. Figure 4, where the tip of this cone is shown, is an example of this situation. It depicts a field of view of 2.9×2.1 mm with a resolution of 12 μm/pixel, corresponding to zone *a* in Fig. 2. This shape would be indicative of a fundamental vibration mode of the ultrasonic transducer. Occasionally, the tip of the cone detaches, forming big droplets of diameters around 500 μm. They quickly fall under the action of gravity. As they can, in any case, be easily filtered, they will not be considered in this study. At a determinate voltage, superimposed on both the whole mass displacement that produces the conical shape and the interfacial waves, a fine mist of small droplets is generated. This process can be seen in Figs. 5 and 6, and could be assimilated to what Boguslaskii and Eknadiosyants (1969) denote as fountain atomization. Both images were taken with the same reso-

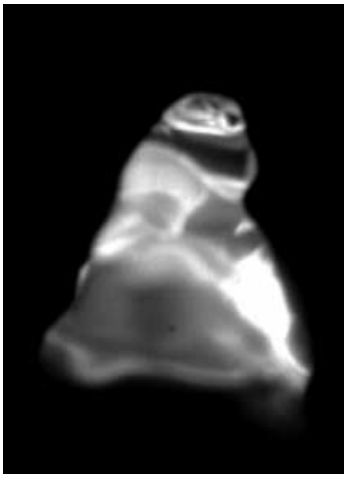

Fig. 4. Conical shape of the perturbed liquid volume for 33 V. Field of view of 2.9×2.1 mm, corresponding to zone *a* in Fig. 2, with a resolution of 12 μm/pixel

Fig. 5. Typical feature of the atomizing results for high voltage where the big cone and a fine cloud of droplets are observed. In this case, the image was obtained recording the laser-induced fluorescence signal of sulforhodamine seeded in the atomized water. The resolution is 5 μm/pixel, a field of view of 1.45×1.9 mm, *zone b* in Fig. 2, and an excitation voltage of 33 V

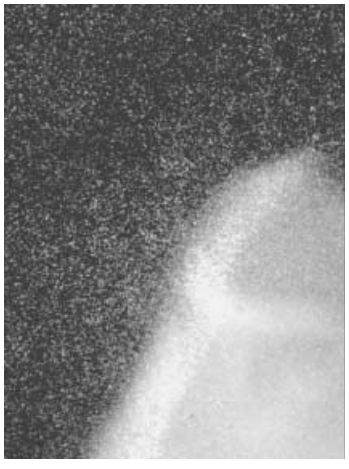

Fig. 6. Another example, for the same conditions as those in Fig. 5

lution of 5 μm/pixel, a field of view of 1.45×1.9 mm, shown as zone *b* in Fig. 2, and an excitation voltage of 33 V. It has to be noted that both images were obtained recording the laser-induced fluorescence of sulforhodamine seeded in the atomized water. This is why the surface waves are barely visible, because laser reflections were eliminated. Although inferring droplet sizes directly from the images can be deceiving, it is obvious that they are substantially smaller than the surface perturbation wavelength. Applying Lang's relation

$$D = 0.34\left(\frac{8\pi\sigma}{\rho F^2}\right)^{1/3} \tag{3}$$

and solving for the operating parameter values, the calculated droplet diameter D is in the range of 3 μm. As will be shown in the next section, this figure is very close to the measurements obtained by laser diffractometry. This coincidence is somewhat surprising, considering the clear divergence between the predicted and the observed surface wavelengths. In Fig. 7, corresponding to a field of view of 1.5×1.5 mm, an excitation voltage of 37 V and a resolution of 2 μm/pixel, the characteristic length of the perturbations on the liquid surface can be compared with the droplet size. The difference is notorious.

In view of the discrepancy between the observed and the predicted surface wavelengths, the origin of the spray droplets might be attributed to cavitation bubbles formed in the liquid/transducer interface. Propagation and collapse of the bubbles would, under this hypothesis, cause the ejection of the fine mist. These bubbles can be identified as the black spots in the bulk of the liquid in Fig. 8a, b, corresponding to a field of view of 0.5×0.75 mm and a resolution of 2 μm/pixel. The imaged area is that denoted by *d* in Fig. 2. The greyscale in the images was chosen so that the bubbles can be discerned simultaneously with the small droplets located over the liquid surface. It is

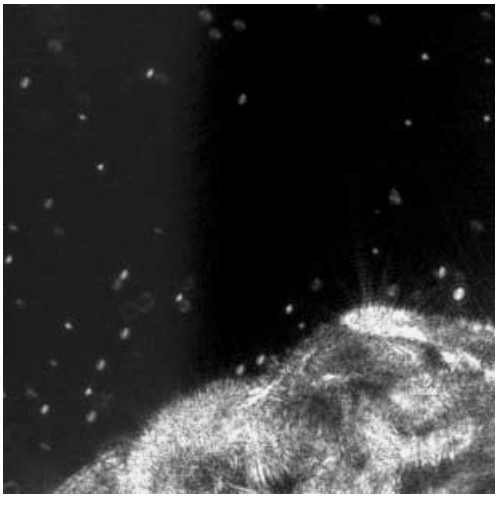

Fig. 7. Perturbed liquid surface, and atomized droplets. Field of view of 1.5×1.5 mm shown as *zone c* in Fig. 2, and a resolution of 2 μm/pixel. Forcing voltage 37 V

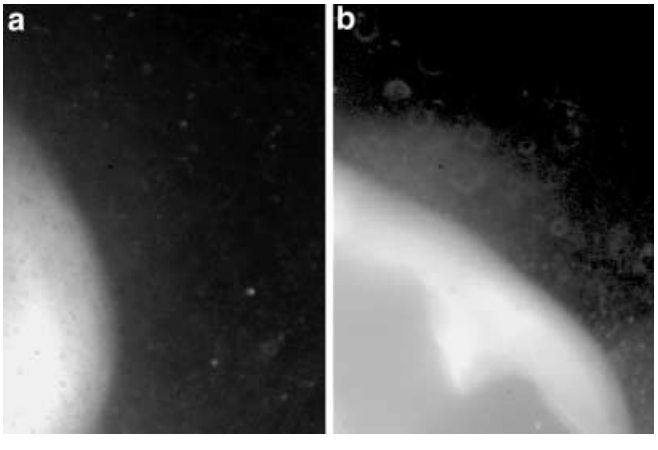

Fig. 8a, b. Images where atomized droplets are visible together with bubbles, corresponding to dark spots, in the interior of the non-atomized water. Field of view of 0.5×0.75 mm, *d* in Fig. 2, and resolution 2 μm/pixel

noticeable that both droplets and bubbles appear to be of similar sizes. Unfortunately, the presence of bubbles has not been systematically observed in all the images in which droplets were detected.

As the discrete water volume is atomized its level over the transducer decreases. When finally there is only a very thin layer, the atomization characteristics change. Instead of forming a relatively homogeneous mist, droplets are formed in straight, parallel streams, and their diameter increases. This behavior is shown in Fig. 9a, b. In both, resolution is 5 μm/pixel, field of view is 1.45×1.9 mm, and the forcing voltage is set to 30 V. In Fig. 9a, a homogeneous cloud is produced over the water surface. In Fig. 9b, however, droplets emerge in coherent streams crossing from right to left in the image. This variation has to be associated with the decrease in both the thickness of the water layer as well as in its curvature.

4.2
Droplet size distributions

In good agreement with previous studies, the droplet size distribution measurements in the present experiments confirm a series of statements that are generally accepted. As stated in Sect. 4.1, the range in which droplet diameters vary is quite reduced, in agreement with Lang's hypothesis relating droplet sizes to ultrasonic frequency. However, the transient measurements in this study reveal that the change in the atomization characteristics described in Fig. 9a, b related to the water level over the transducer, is accompanied by the appearance of a second peak of larger droplets in the size distribution function.

If a constant water level is maintained over the ceramic disk, the distribution does not change with time. This can be observed in Fig. 10, corresponding to an excitation voltage of 32.5 V. The axes in the plot represent droplet diameter (logarithmic), and percentage in volume of the atomized liquid corresponding to each diameter class.

At this point, it must be noted that the distribution function actually represents a histogram with bins of a width that is not constant. On the contrary, it increases exponentially with the diameter. For this reason, plotting the histogram in logarithmic coordinates gives a direct indication of the liquid volume percentage in each bin as if they were equal.

In Fig. 10, a main peak is clearly located around 3.5 μm. A secondary peak is observed in some measurements of about 5.2 μm. A final rise is also observed in the 60–70-μm region, which can be related mainly to break up due to the displacement of the liquid volume as a whole, not directly related to the ultrasonic frequency.

When the water mass initially deposited over the transducer is allowed to be atomized in its entirety, the temporal evolution reveals a change in the nebulization conditions. Figure 11a–d shows temporal evolutions for different excitation voltages (35, 40, 42.5, and 45 V). Initially, a distribution similar to that described in Fig. 10 is observed. However, as time progresses, the distribution evolves. The initial double peak with the principal maximum in 3.5 μm and the secondary at 5.2 μm tend to merge into a single one located at 5.2 μm. As time advances, this peak displaces towards larger diameters, reaching values as high as 9 μm in Fig. 11d. At the same time, a third peak located in the 60–70-μm range increases at the expense of the one corresponding to 3–5 μm. This effect is especially noticeable in Fig. 11a, b, corresponding to 35 and 40 V

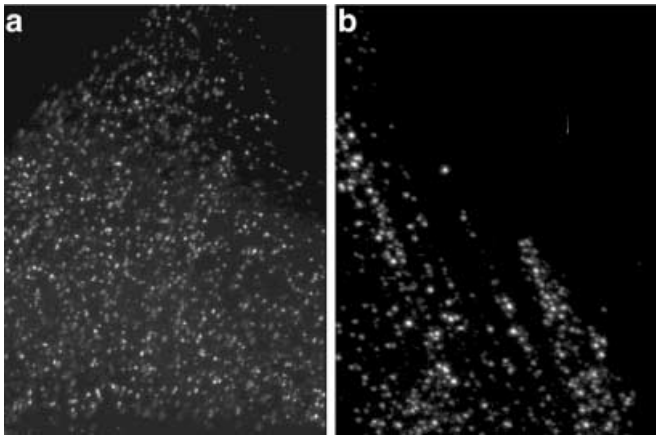

Fig. 9a, b. Atomization characteristics for different water levels over the transducer: **a** with an approximate volume of 0.2 ml; **b** in the final stages of the process with only a thin layer of liquid on the disk surface. In both images, resolution is 5 μm/pixel, field of view is 1.45×1.9 mm as depicted in *zone b* in Fig. 2, and the forcing voltage was set to 30 V

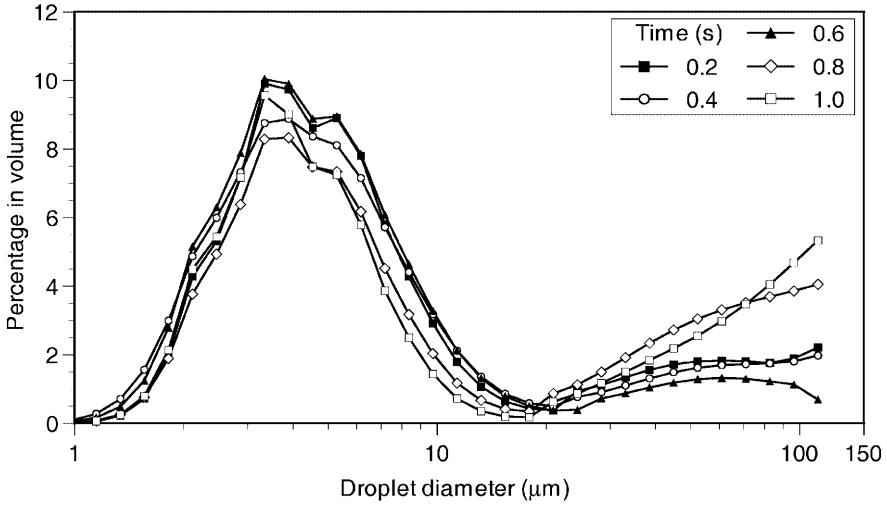

Fig. 10. Temporal evolution of the droplet size distribution for a fixed liquid level over the transducer and a forcing voltage of 35 V. Note the logarithmic scale in the droplet diameter axis

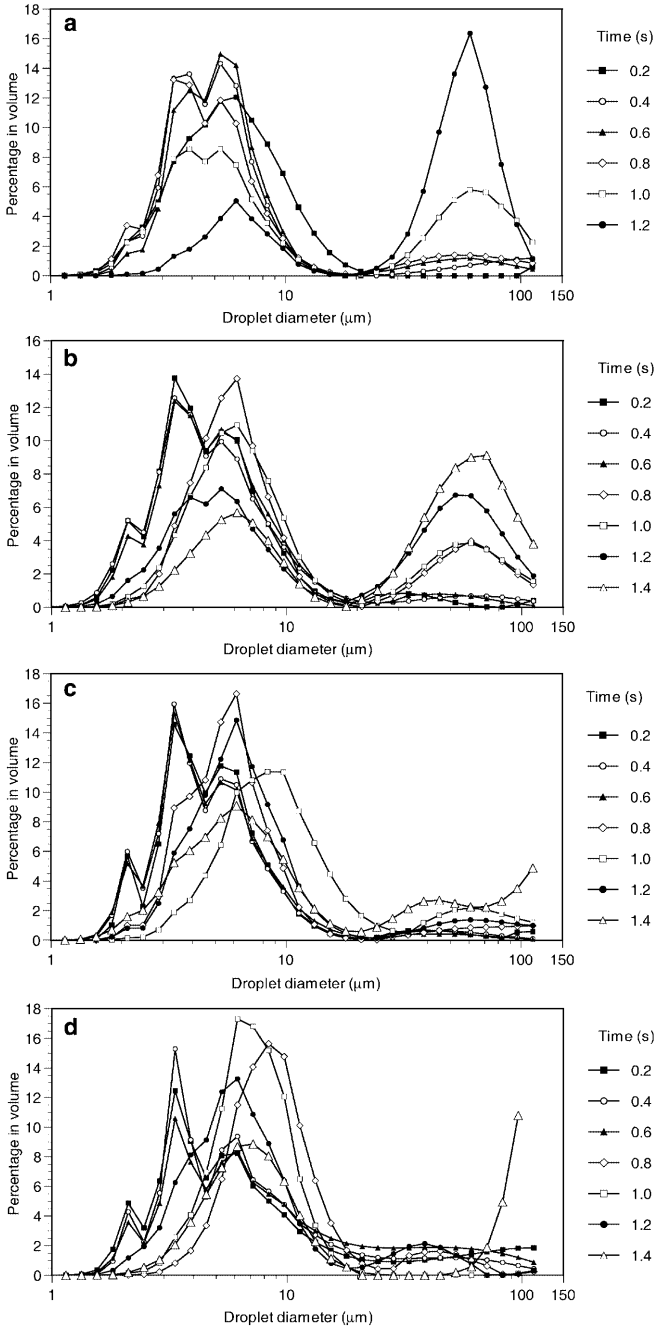

Fig. 11a–d. Temporal evolution of the droplet size distribution for the atomization of a small amount of water deposited over the transducer without further addition of liquid. Forcing voltage: **a** 35 V; **b** 40 V; **c** 42.5 V; **d** 45 V

respectively. As a final observation, a small peak located at 2 μm can also be discerned at the initial atomization stages. In most measurements, this peak disappears after 0.6 s. In any case, the size dependence on voltage is relatively weak.

To analyze the droplet size distribution variation with voltage, measurements were obtained atomizing with a constant water level, to eliminate the temporal dependence. Results are presented in Fig. 12. The distribution is similar to those presented in Fig. 11. It is interesting to observe that, for voltages below 40 V, all the distributions

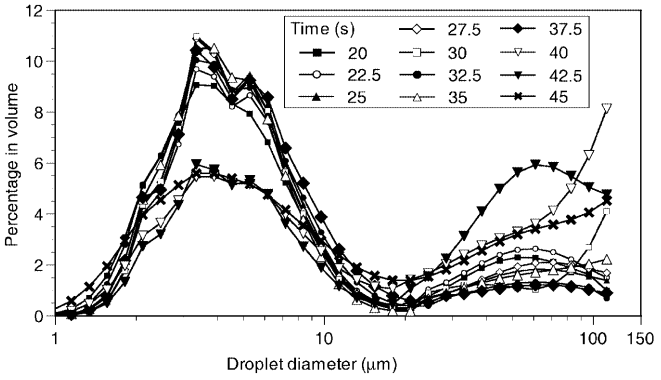

Fig. 12. Variation in the droplet size distribution with voltage. Measurements were obtained atomizing with a constant water level, to eliminate the temporal dependence

are very similar, again corroborating the relative independence between droplet size and forcing amplitude. For the higher voltages, the secondary peak increases its relative importance. Formation of these larger droplets could be caused by the more violent vibration of the transducer, probably independent of the specific ultrasonic frequency. Tests should be conducted using other transducers with different resonance frequencies to corroborate this hypothesis.

It has to be remarked that, although droplet size is mainly dependent on frequency, the rate at which liquid is atomized is mostly controlled by the driving voltage. This is confirmed by the measurements shown in Fig. 13, obtained registering the time needed to nebulize a fixed water volume. Atomization rate clearly increases with voltage. It has to be noted that if droplet generation is attributed to detachment from surface wave crests, once the amplitude is high enough so that droplets are ejected from each crest, the rate at which they are formed, together with their size, would reach a constant value determined only by the oscillation frequency. A further increase in the nebulization rate could only be explained by an increase in the liquid surface area from which the droplets emerge. If cavitation mechanisms are employed to justify this dependence, the

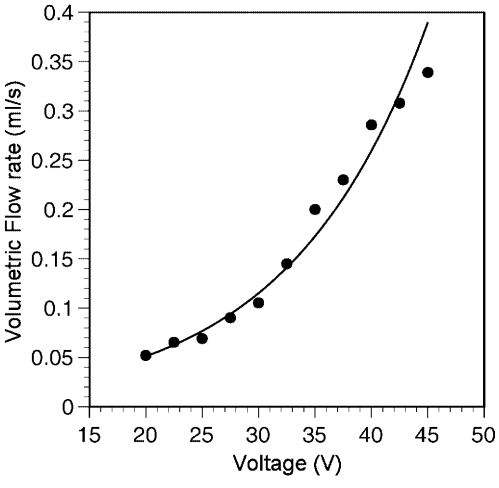

Fig. 13. Atomization rate as a function of voltage

explanation is easier, because larger-oscillation amplitudes will cause higher pressure variations favoring the formation of cavitation bubbles (Söllner 1936b).

From the size distributions, some statistical parameters were calculated. Mean diameter, D_{10}, and mass mean diameter, D_{30}, both of them based on number of droplets, as a function of the forcing voltage are presented in Fig. 14. The same plot also includes 10% and 50% volume percentiles, $D_{v0.1}$ and $D_{v0.5}$. Only $D_{v0.5}$ shows an abrupt increase for voltages over 37.5 V due to the higher relative weight given to large droplets. This increase is correlated with the change in the distribution curves displayed in Fig. 12 already discussed. In spite of that, it is remarkable that for voltages between 22.5 and 37.5 V, even the 50% percentile is located below 6 μm. For temporally evolving atomization, a diameter increase is observed for the final stages, when almost all the water is nebulized. An example is shown in Fig. 15, corresponding to an excitation of 42.5 V. The diameter increase at 1 s could be due to some occasional splashing.

A final parameter was also analyzed: the volume fraction of droplets with diameter below 5 μm. This parameter would determine, for example, whether a nebulizing device is acceptable for asthma inhalation therapy (for this application, a minimum of 30% is typically required). Figure 16 shows the obtained results for stationary atomization. In agreement with the results of Fig. 14, the fraction remains almost constant for voltage values below 37.5 V, with a value around 60%. For higher voltages, the fraction of large droplets increases, as shown in Fig. 12, and the percentage below 5 μm drops to 30%.

4.3 Velocity measurements

Image pairs were acquired with a spatial resolution of 2 μm/pixel, extending the imaged area from 2.5 to 4 mm above the transducer surface (dotted square in Fig. 2). In this case, a discrete water volume was atomized yielding a constant decrease in its level over the transducer. Three different scenarios are observed in the images: one where only the liquid mass is visible, a second one in which the liquid surface and droplets coexist in the same picture, and a third situation where only droplets are visible. The first one does not provide information about droplet velocity. The third group of images can also correspond to two different situations: droplets that just emerged from the liquid surface, or a cloud that floats in the air at very low velocity after nearly all the liquid volume was atomized. Some results are displayed in Fig. 17a–c, corresponding to a forcing voltage of 22 V. The dark region in the lower part of Fig. 17a corresponds to non-atomized water. In these images, velocities vary from 15 cm/s to 4 cm/s.

Figure 18 shows the mean velocity for each image averaged over 15 images, for different voltages. The primary interest of the PIV measurements was to determine the droplet exit velocity. With the present experimental setup,

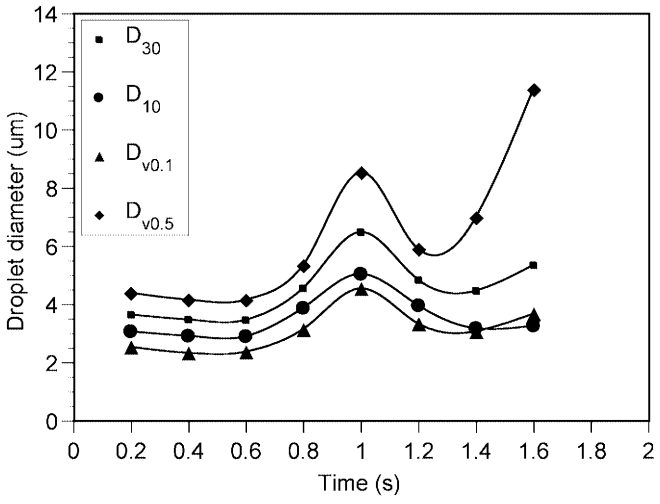

Fig. 15. Temporal evolution of the statistical parameters in Fig. 14 when atomizing a fixed amount of liquid. Forcing voltage 42.5 V

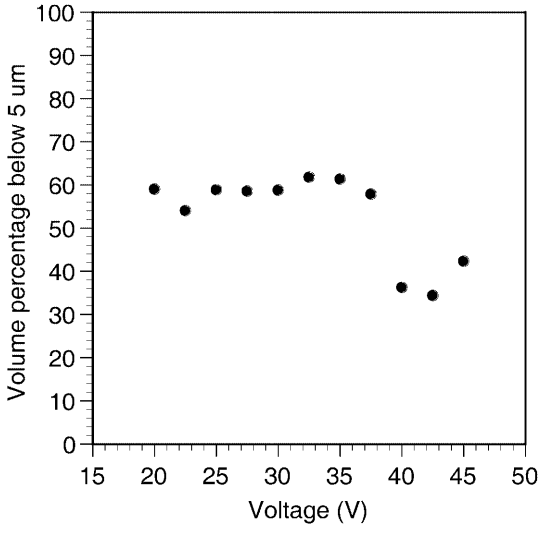

Fig. 16. Volume fraction of droplets with diameter below 5 μm as a function of the excitation voltage for stationary atomization

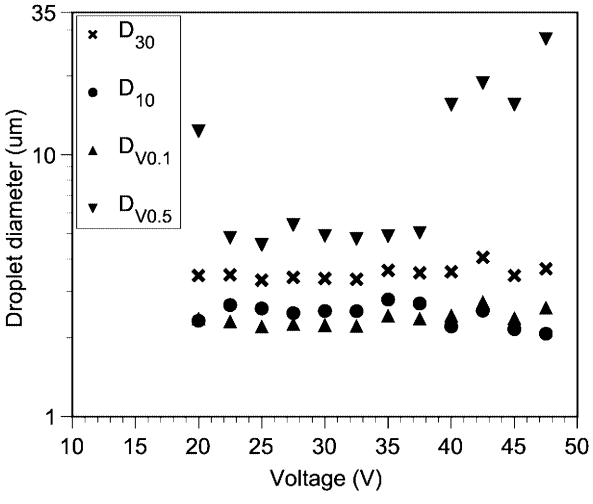

Fig. 14. Mean diameter, D_{10}, mass mean diameter, D_{30}, 10% and 50% volume percentiles, $D_{v0.1}$ and $D_{v0.5}$, as a function of the forcing voltage. All these parameters were derived from the distributions in Fig. 11

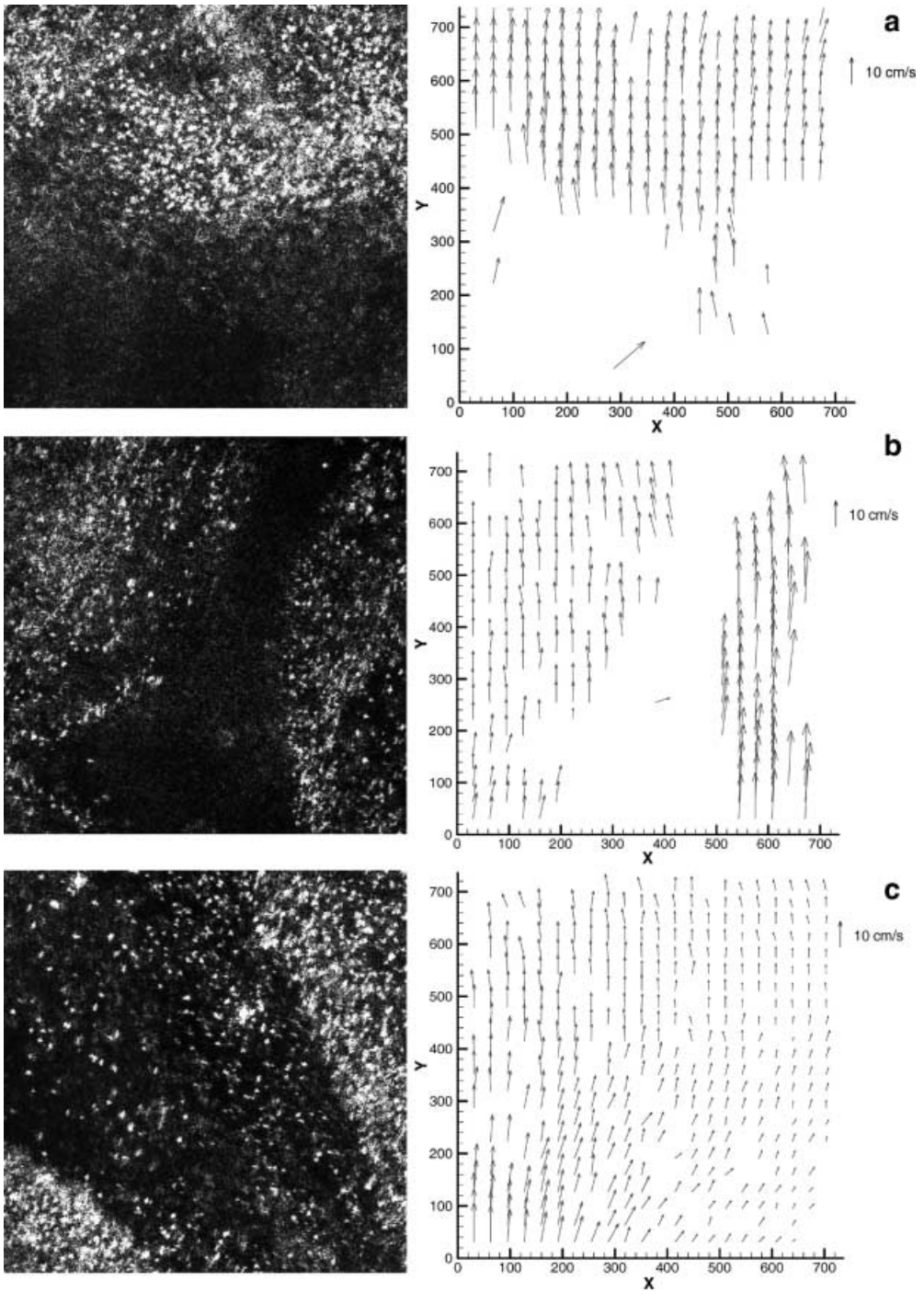

Fig. 17a–c. Images of droplets together with corresponding velocity maps. The imaged area, zone *c* in Fig. 2, is 1.5×1.5 mm with a spatial resolution of 2 μm/pixel

if droplets were only decelerated by gravity effects, a 4 μm droplet ejected vertically with a velocity of 20 cm/s would come to a stop in only 2 mm, although it is obvious that in the real situation, aerodynamic effects cannot be neglected. In these experiments, care was taken to avoid air flows in the air surrounding the transducer. Therefore, it was estimated that to obtain a better indication of the ejection velocity it would be more convenient to take the 15-image average of the maximum values in each image. The maximum values among these maxima are also included in the plot. From the three curves depicted, it can be concluded that the droplet velocity increases with voltage.

5 Conclusions

Ultrasonic water atomization at MHz frequencies was studied. Experiments were performed both maintaining a constant water level over the piezoceramic transducer and leaving a fixed liquid volume to be atomized completely. In this way, the temporal evolution of the process was analyzed. It was confirmed that the droplet size distribution is relatively independent of the forcing voltage. For the oscillation frequency in the present measurements, 1.65 MHz, the droplet size distribution function presents a main peak between 3 and 5 μm. However, at high voltages,

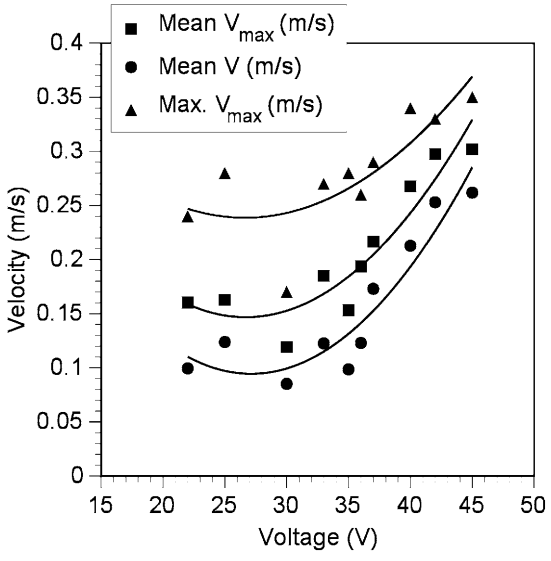

Fig. 18. Droplet velocity as a function of excitation voltage. Mean V_{max} is the average over several images of the maximum velocity values in each image. Max V_{max} is the maximum values of the maxima

violent movement of the bulk of the liquid due to the large forcing amplitude displaces the droplet distribution towards a secondary maximum, corresponding to larger diameters on the order of 60 μm.

The atomization process occurs according to the following sequence. The ultrasonic vibration of the ceramic disk causes the oscillation of the liquid mass that forms a cone, and the appearance of surface waves in the air/liquid interface. Their wavelength, however, was observed to be larger than that predicted by Rayleigh's equation. In some images, the presence of bubbles in the bulk of the liquid was detected. They are most probably due to cavitation at the disk/water interface and could also be responsible for the whole atomization process. Droplet formation only occurs for amplitude oscillations over a certain threshold, corresponding to forcing voltages above 15 V.

For the final atomization stages, when the water over the transducer is almost depleted, the spatial distribution of the droplet cloud changes. Instead of a homogeneous mist, droplets emerge in discrete filaments. This is accompanied by an increase in the droplet diameter, caused both by a displacement of the peak diameter towards higher values (from 3 μm to nearly 9 μm) and the presence of a second peak at around 50 μm. This effect is associated with the decrease in the surface curvature.

It was also determined that both the atomization rate and the droplet exit velocity increase with the forcing voltage.

References

Bassett JD, Bright WW (1976) Observations concerning the mechanism of atomization in an ultrasonic fountain. J Aerosol Sci 7:47–51

Bendig L (1988) New developments of ultrasonic atomizers. In: Proceedings of the 4th International Conference on Liquid Atomization and Sprays Systems. The Fuel Society of Japan, Tokyo, pp 133–138

Benjamin TB, Ursell F (1954) The stability of the plane free surface of a liquid in vertical periodic motion. Proc R Soc London A 225:505–515

Bisa K, Dirnagl K, Esche R (1954) Zerstäubung von Flüssigkeiten mit Ultraschall [Ultrasonic spraying of liquids], Siemens-Z 28:341–344

Boguslaskii YY, Eknadiosyants OK (1969) Physical mechanism of the acoustic atomization of a liquid. Sov Phys Acoust 15:14–21

Chiba C (1975) Atomization of liquid by inmersed and convergent ultrasonic vibrators (case of distilled water). Bull J Soc Mech Eng 18:376–382

Edwards WS, Fauve S (1994) Patterns and quasi-patterns in the Faraday experiment. J Fluid Mech 278:123–148

Eisenmenger W (1959) Dynamic properties of surface tension of water and aqueous solutions of surface active agents with standing capillary waves in the frequency range from 10 kHz to 1.5 MHz. Acoustica 9:327–340

Eknadiosyants OK (1968) Role of cavitation in the process of liquid atomization in an ultrasonic fountain. Sov Phys Acoust 14:80–84

Faraday M (1831) On the forms and states assumed by fluids in contact with vibrating elastic surfaces. Phil Trans R Soc London 52:319–340

Fogler HS, Timmerhaus KD (1965) Ultrasonic atomization studies. J Acoust Soc Am 39:515–518

Gershenzon EL, Eknadiosyants OK (1964) The nature of liquid atomization in an ultrasonic fountain. Sov Phys Acoust 10:127–132

Kelvin Lord (W Thomson) (1871) Hydrokinetic solutions and observations. Phil Mag 42:362–377

Lang RJ (1962) Ultrasonic atomization of liquids. J Acoust Soc Am 34:6–8

Miles J (1994) Faraday waves: rolls versus squares. J Fluid Mech 269:353–371

Peskin RL, Raco RJ (1963) Ultrasonic atomization of liquids. J Acoust Soc Am 35:1378–1381

Rayleigh L (1883) On the crispation of fluid resting upon a vibrating support. Phil Mag 15:50–58

Rayleigh L (1917) On the pressure developed in a liquid during the collapse of a spherical cavity. Phil Mag Ser 6 34:94–98

Sindayihebura D, Bolle L (1998) Ultrasonic atomization of liquid: stability analysis of the viscous liquid film free surface. Atomiz Sprays 8:217–233

Sindayihebura D, Cousin J, Dumouchel C (1997) Experimental and theoretical study of sprays produced by ultrasonic atomizers. Part Part Syst Charact 14:93–101

Söllner K (1936a) The mechanism of the formation of fogs by ultrasonic waves. Trans Faraday Soc 32:1532–1536

Söllner K (1936b) Experiments to demonstrate cavitation caused by ultrasonic waves. Trans Faraday Soc 32:1537–1538

Sorokin VI (1957) The effect of fountain formation at the surface of a vertically oscillating liquid. Soviet Phys Acoust 3:281–291

Topp MN (1973) Ultrasonic atomization – a photographic study of the mechanisms of disintegration. Aerosol Sci 4:17–25

Wood WR, Loomis AL (1927) The physical and biological effects of high frequency sound-waves of great intensity. Phil Mag 4:417–437